

Compact multi-fringe interferometry with sub-picometer precision

Katharina-Sophie Isleif,* Gerhard Heinzl, Moritz Mehmet, and Oliver Gerberding†
*Max Planck Institute for Gravitational Physics (Albert Einstein Institute)
and Leibniz Universität Hannover
Callinstr. 38, 30167 Hannover, Germany*

(Dated: March 8, 2019)

Deep frequency modulation interferometry combines optical minimalism with multi-fringe readout, precision however is key for applications such as optical gradiometers for satellite geodesy or as dimensional sensor for ground-based gravity experiments. We present a single-component interferometer smaller than a cubic inch. Two of these are compared to each other to demonstrate tilt and displacement measurements with a precision of less than $20 \text{ nrad}/\sqrt{\text{Hz}}$ and $1 \text{ pm}/\sqrt{\text{Hz}}$ at frequencies below 1 Hz.

I. INTRODUCTION

The highly precise measurement of distance variations with laser interferometry is one of the core tools of experimental gravitational physics and dimensional metrology. A prime example is the detection of gravitational waves by the LIGO and Virgo detectors sensing $1 \text{ am}/\sqrt{\text{Hz}}$ over 4 km using homodyne interferometry [1]. Sensing with this precision is however only possible for interferometers locked to a particular operating point within a tiny fraction of one fringe. In contrast to this, space-based gravity experiments typically require multi-fringe interferometry between free-floating test masses (TMs). State-of-the-art for such missions is high dynamic-range heterodyne interferometry [2], as developed for the space-based gravitational wave detector LISA [3]. Its precursor mission LISA-Pathfinder (LPF) has demonstrated the readout of TM displacements and tilts with precisions of $30 \text{ fm}/\sqrt{\text{Hz}}$ and better than $20 \text{ nrad}/\sqrt{\text{Hz}}$, respectively, at frequencies below 1 Hz [4]. The heterodyne concept however imposes challenges in terms of its scalability, particularly if one desires to increase the number of TMs and the degrees of freedom (DoF) to be read out. Optical gradiometer satellite missions for example require the readout of six TMs, each with several DoF to improve on current sensitivities [5, 6]. Other metrology applications and experiments might also benefit from LPF-level displacement sensing, if available in a compact and up-scalable format.

Various interferometer concepts have been studied with the aim of reducing the optical complexity of heterodyne interferometers while preserving the performance [7]. Self-homodyning interferometer techniques with phase-shift keying methods like digital interferometry [8], deep phase modulation [9, 10] or deep frequency modulation interferometry (DFMI) [11–13] are attractive candidates that reduce the optical complexity at the expense of more complex phase extraction algorithms. In recent years many proof-of-principle studies [13–18] have

revealed greatly simplified optical readout schemes that rely on such hybrid approaches. Effectively they combine continuous-wave laser sources with specific modulations to create pulsed- or comb-like fields that enable optical simplification, phase readout and sometimes even multiplexing. However, probing and achieving the low-frequency noise required for future gravity experiments has remained rare for these techniques [18].

We have focused on studying DFMI, a technique that has recently gained wide interest [19–22]. It uses a single laser beam that is strongly modulated sinusoidally in its frequency. By injecting this light into an interferometer with unequal arms we generate an output pattern that contains complex amplitudes at the modulation frequency and its higher harmonics. The essence of DFMI, as we use it, is the phase extraction algorithm: We employ a non-linear fit algorithm based on a Levenberg-Marquardt (least squares) routine. It uses a Bessel function decomposition of the complex amplitudes at the modulation frequency and its first, about ten, harmonics [10]. This allows us to extract four fundamental measurement parameters in real-time: the interferometric phase φ and amplitude, the modulation index m and the modulation phase. The effective modulation index depends on the frequency modulation (FM) deviation, Δf , and on the interferometer arm length mismatch, ΔL , and is given by the relation $m = 2\pi\Delta f\Delta L/c_0$, with the speed of light c_0 . This allows us to build compact optical set-ups by increasing the FM deviation. Estimates of absolute distances are also possible with this readout scheme by tracking the modulation index m [11]. Compared with the classic heterodyne scheme or Homodyne Quadrature Interferometry [23], DFMI requires less optical components which allows for more compact layouts without giving up the multi-fringe capabilities. While previous studies have verified this functionality [13], we present an experiment that demonstrates the actual displacement sensing performance of DFMI on the $1 \text{ pm}/\sqrt{\text{Hz}}$ -level for the first time, making it an attractive alternative to heterodyne interferometry.

* katharina-sophie.isleif@aei.mpg.de

† contact@olivergerberding.com

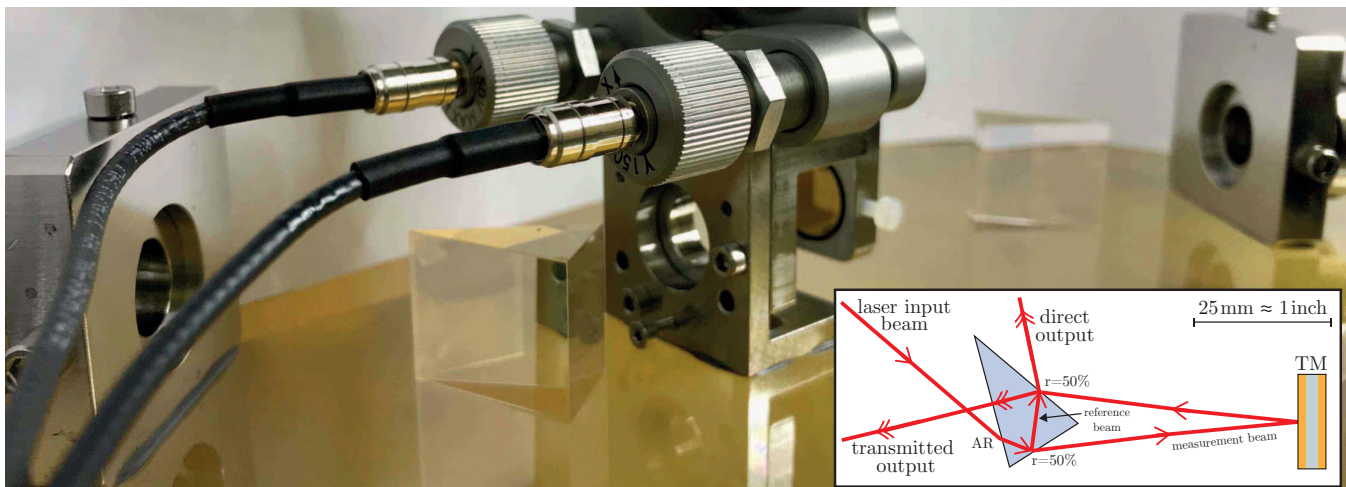


FIG. 1. Photograph of the Test Mass in the Middle (TMitM) experiment. One prism is placed on both sides of the gold-coated mirror (12.7 mm in diameter), which is suspended from a three-axes piezo actuator. Titanium fiber collimators fixed in Invar holders provide light to each interferometer. The inset shows a sketch of the left prism-shaped interferometer with beam splitter and anti-reflective (AR) coating. The laser beam paths are drawn in red and hit the test mass (TM) under 4.1° .

II. EXPERIMENT

A single-component, prism-shaped, compact interferometer was designed by using the optical simulation tool IFOCAD [24]. It has a triangular base surface with two equal sides of 25 mm length. A sketch of the component is shown in inset of Fig. 1; the laser propagation is drawn in red. The first optical surface has an anti-reflective coating, the second surface has a beam splitter coating with 50% reflectivity, such as the third surface, which is used for recombining reference and measurement beam. The reference beam travels a short distance inside the medium while the measurement beam leaves the medium and is reflected by a TM which is placed next to the prism. The interferometer is designed for an angle of incidence of 4.1° under which the measurement beam hits the TM. The interferometer provides two redundant optical output ports which we call *direct* and *transmitted*. The transmitted port contains the interference signal with a phase shift of π with respect to the direct one. The transmitted beams also leave the medium without compensating the previous refraction which leads to beam profile distortions in the transmitted port and an effective ellipticity of about 0.7 for both interfering beams.

A. Optical set-up

We constructed a quasi-monolithic optical testbed, the so-called Test Mass in the Middle (TMitM) experiment (Fig. 1). It consists of a 4 mm thick mirror that is gold-coated on both sides and mounted on a three-axis piezo-transducer (PZT) that is glued in the center of an optical bench (OB), which is made of the glass-ceramic Clearceram with a low coefficient of thermal expansion

of $1 \cdot 10^{-8} / \text{K}$. A prism is glued with UV cured adhesive onto the OB on each side of the TM. Two adjustable fiber output couplers provide the laser light for the prisms. The point-symmetry of the set-up allows us to perform two redundant interferometric measurements of the same TM motion. Both interferometers are aligned such that after vacuum chamber evacuation we achieve maximum contrast (more than 95%), taking into account a small alignment change due to the refractive index of air.

Fig. 2 shows a sketch of the experiment and its infrastructure. As illustrated in inset (a), the laser source is a fiber-coupled external cavity diode laser (ECDL) with a center wavelength of $\lambda = 1064 \text{ nm}$ that is modulated by $\Delta f \approx \pm 5 \text{ GHz}$ with a rate of $f_m = 0.8 \text{ kHz}$. It provides 15 mW optical power that is routed into a vacuum chamber (shown in inset (b)). A polarization maintaining fiber splitter equally distributes the light inside the chamber via four ports to a power monitor, the TMitM experiment and a quasi-monolithic interferometer which is used as frequency reference. This optical reference allows us to measure the FM deviation and the laser frequency noise accumulated over 7 cm arm length mismatch and to stabilise both [25]. Amplitude fluctuations, caused by the strong frequency modulation and polarisation fluctuations in the fibers, are actively stabilised by a closed loop control of the laser diode current with 100 kHz unity gain frequency.

The effective modulation index differs between the three interferometers due to their individual arm length mismatches and is $m_{\text{REF}} = 7.5 \text{ rad}$ (stabilised) in the reference interferometer, $m_L \approx 8.9 \text{ rad}$ in the left and $m_R \approx 9.1 \text{ rad}$ in the right prism interferometer.

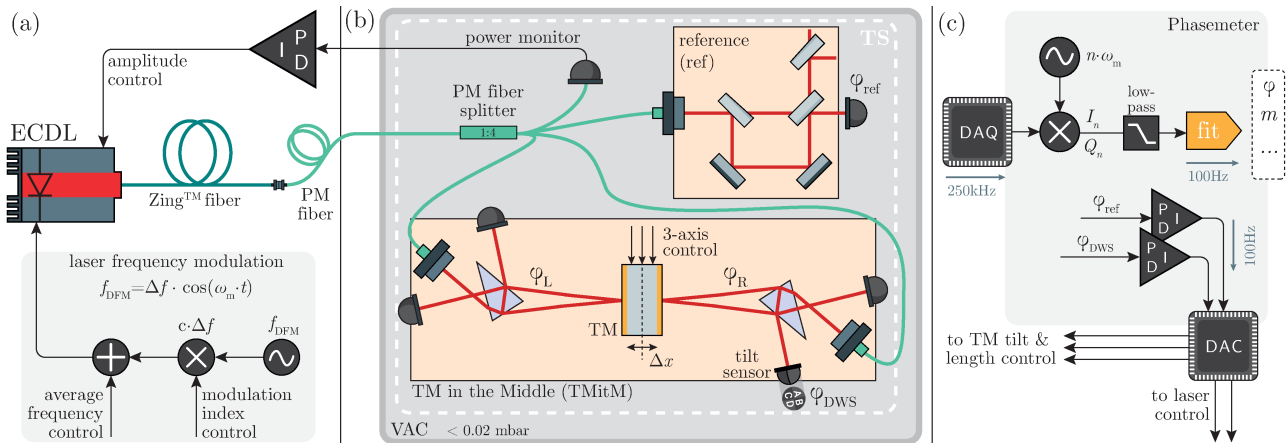


FIG. 2. Sketch of the experiment. Inset (a) shows the laser preparation. A deep frequency modulation, f_{DFM} , is applied to a fiber-coupled external cavity diode laser (ECDL). All fiber components are polarisation maintaining (PM). The vacuum chamber (VAC), shown in inset (b), houses a thermal shielding (TS) which covers two quasi-monolithic interferometers: the reference (ref) and the Test Mass in the Middle (TMitM). The data acquisition (DAQ) system has eight analogue inputs which are simultaneously digitised and processed in a software phasemeter, both shown in inset (c). Analogue control voltages are provided by a digital-to-analogue converter (DAC) and are used to actuate on the laser and test mass (TM).

B. Readout

The readout algorithm of DFMI is briefly illustrated in Fig. 2(c). For the given modulation indices between 7 and 9 rad, we observe up to 10 higher harmonics of the modulation rate in the pattern. The extraction of the desired fit parameters is done in real-time in the *phasemeter* which is implemented in a C-program running on a PC. An 8-channel data acquisition card with 250 kHz sampling rate is used to digitise the photodiode voltages, which were generated from the photo currents via transimpedance amplifiers. A digital-to-analogue converter provides actuation signals from the phasemeter via a USB interface. Five digital feedback control loops (proportional-integral controllers) are integrated in software: The tilt of the TM in horizontal and vertical direction can be controlled by actuating on the three-axis PZT mount. As error signal we use a differential wavefront sensing (DWS) measurement which is provided by a quadrant photodiode (QPD). The coupling factor between optical tilt and DWS signal of about 5000 rad/rad was calculated by means of optical simulations for an assumed beam waist radius of 0.5 mm and a waist position of 100 mm; lenses with 25.4 mm focal length produced a spot size radius of 0.12 mm on the diodes' active area. The experimental data verified this coupling factor. The pathlength of the TM is controlled by actuating on all three PZT axes simultaneously. The two remaining feedback loops control the average laser frequency and its applied FM deviation by tuning the modulation DC voltage and AC amplitude, respectively. The software phasemeter restricts the bandwidths of all controls to about 10 Hz.

III. RESULTS

The TMitM experiment measures two interferometric phases, φ_L and φ_R , on the left and on the right side of the TM. The wavenumber $k = 2\pi/\lambda$ converts the phases into displacements, $\tilde{x} = \varphi/k$, and we can define \tilde{x}_L and \tilde{x}_R for both sides, and equivalent \tilde{x}_{ref} for the reference interferometer. A TM motion, Δx , is monitored redundantly in both prism interferometers except for an opposite sign. We introduce the parameter ε which adds an additional noise term that is not common mode in the two interferometers. If one also includes laser frequency noise, ν , it couples into all interferometers scaled by their arm length difference, given by m_L , m_R , m_{ref} , as extracted by the phasemeter. The displacement noise for each interferometer can be described by:

$$\tilde{x}_L = +2\Delta x + \nu \cdot m_L, \quad (1)$$

$$\tilde{x}_R = -2\Delta x + 2\varepsilon + \nu \cdot m_R, \quad (2)$$

$$\tilde{x}_{ref} = \sigma + \nu \cdot m_{ref}. \quad (3)$$

The test mass displacement, Δx , occurs amplified by a factor of 2 in each prism measurement due to the reflection set-up. With an angle of incidence of about 4.1° this results in a coupling factor of nearly 2 which is inserted in the equations above. The measurement of the reference interferometer contains an additional phase noise term, σ , that is driven by e.g. wrong polarizations or other noise influences unique to this interferometer [25]. Eqs. (1)-(3) can be combined to two expressions:

$$\tilde{x}_{TM} := (\tilde{x}_L - \tilde{x}_R)/4 = \Delta x + \varepsilon/2, \quad (4)$$

$$\tilde{x}_{RPN} := (\tilde{x}_L + \tilde{x}_R - \tilde{x}_{ref} \cdot \rho)/4 = \varepsilon/2 + \sigma \cdot \rho/4, \quad (5)$$

with $\rho = (m_L + m_R)/m_{ref}$. Eq. (4) contains the actual TM motion and the noise term ε . Eq. (5) combines

all three measurements to reveal the total residual phase noise (RPN), containing only the two noise terms σ and ϵ . The RPN can be used to analyse any residual noise in the testbed or of the readout technique itself. A further signal combination is the opto-electronic noise, \tilde{x}_{OEN} , that shows the difference of two redundant outputs of a recombination beam splitter, e.g. $\tilde{x}_{\text{L,direct}} - \tilde{x}_{\text{L,transmitted}}$, which is a useful quantity for the evaluation of readout or stray light noise in the experiment.

The result of the TM displacement noise is plotted in Fig. 3. By applying all control schemes (laser frequency/modulation and TM stabilization) we are able to sense TM displacements with $230 \text{ fm}/\sqrt{\text{Hz}}$ precision between 300 mHz and 10 Hz (\tilde{x}_{RPN}). The TM motion, \tilde{x}_{TM} , shows artefacts at higher harmonics that are induced by acoustic and seismic noise. The peak at 25 Hz was identified to be the oscillation of the vacuum pump running during this measurement. At frequencies below 30 mHz the noise increases with a $1/f^2$ -behaviour. The reasons for this are to some extent temperature fluctuations that cause beam jitter, or other non-linear effects.

A. Non-linearities

Amplitude fluctuations couple into the opto-electronic noise, \tilde{x}_{OEN} , and might be caused by the laser source itself or due to polarisation fluctuations. The amplitude stabilisation reduces this noise up to a bandwidth of 100 kHz. Digitisation noise limits \tilde{x}_{OEN} at $150 \text{ fm}/\sqrt{\text{Hz}}$ down to 30 mHz, as shown in Fig. 3. We assume that polarisation fluctuations caused by refractive index changes in the fiber components are the main reason for the increasing noise level below 30 mHz. A residual amplitude modulation caused by the applied strong frequency modulation, and not sufficiently suppressed by the stabilisation, cannot be excluded either.

The reference interferometer is used as sensor to stabilise the laser frequency noise and to lock the modulation index to a constant value, here $m_{\text{ref}} = 7.5 \text{ rad}$. The stabilisation of the modulation index is useful to lock the operation point of the laser. While the control of the modulation index did not show any significant improvements in the phase performance, we are able to reduce laser frequency noise drifts below the unity gain frequency of 10 Hz. By subtracting the remaining laser frequency noise in data post-processing, we are able to further improve the performance between 100 mHz and 50 Hz by one order of magnitude at 1 Hz. The resulting residual phase noise, is given by \tilde{x}_{RPN} in Fig. 3. It is limited by opto-electronic noise above 1 Hz and by some unexplained non-common mode noise source below this frequency. Despite this excess noise the measurement shows that DFMI with single-component interferometers is able to achieve 1 pm-level precision comparable to, and partly better than, previous breadboard experiments for LISA and LPF [7, 26–28].

The measurement also shows a dynamic range of more

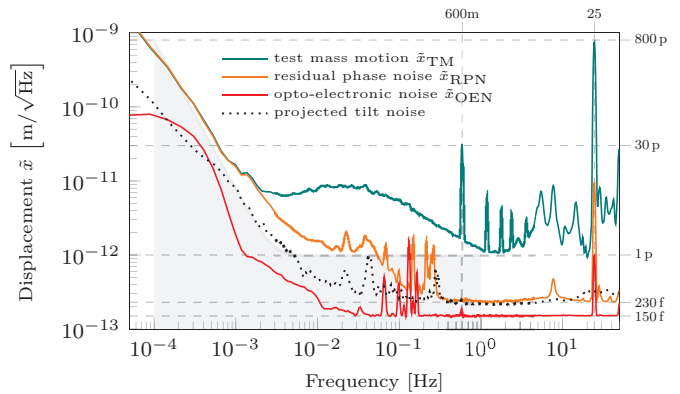


FIG. 3. Displacement performance of DFMI. As reference we plot the sensitivity curve of the LISA mission concept document of $1 \text{ pm}/\sqrt{\text{Hz}}$ relaxed to frequencies below 3 mHz as grey area [3]. The individual signals are calculated from the interferometric phases according to Eqs. (4) and (5).

than two orders of magnitude at 600 mHz between \tilde{x}_{TM} and \tilde{x}_{RPN} , and almost three orders of magnitude at 25 Hz. Residual readout non-linearities might be caused by the strong frequency modulation itself that could limit the dynamic range capabilities, as discussed in previous studies [11, 13]. Possible reasons are harmonic distortions of the modulation caused by the function generator or the laser itself via the external cavity excitation. In the current range these effects do not seem to be limiting, however, they might become dominant for higher dynamics if no further compensation is applied. The influence of non-flat transfer functions of the photo-receivers was also measured and corrected and is most probably not the limiting factor at this point. Other geometrical effects, like non-parallel incidence or a wedge of the TM, can also lead to non-linear couplings. The current noise limitations are however more likely explained by undesired tilts as described in the following.

B. Tilt-to-length noise

In a subsequent measurement we used a second QPD in the other prism interferometer and monitored the out-of-loop behaviour of TM tilts. Due to the limited number of readout channels we were not able to stabilise the laser frequency and modulation nor the TM path-length during this additional measurement. Only the TM tilt noise was monitored and the according in- and out-of-loop measurements are shown in Fig. 4. We are able to stabilise the TM tilt down to noise levels on the order of $20 \text{ nrad}/\sqrt{\text{Hz}}$ above 40 mHz, as the out-of-loop measurements indicate. The projected TM displacement noise can be determined by combining the left and right tilt measurements (in- and out-of-loop). The DWS and tilt-to-length coupling factors for beam jitter

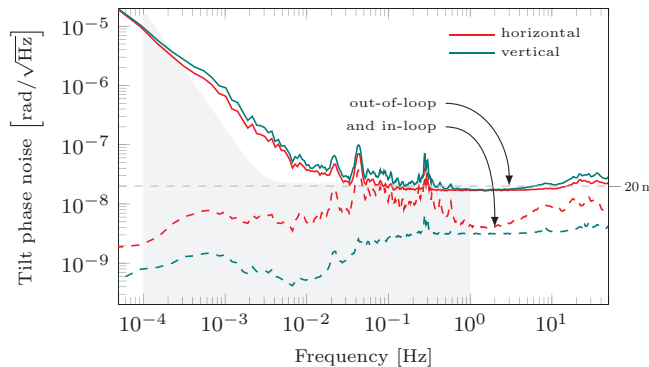


FIG. 4. Tilt noise performance of DFMI. As reference we plot the mission requirements of the LPF test campaign of $20 \text{ nrad}/\sqrt{\text{Hz}}$ relaxed to frequencies below 3 mHz as grey area [29]. To get the optical tilt noise performance we divided the measured DWS phase measurement by the coupling factor ($\approx 5000 \text{ rad/rad}$).

were determined by optical simulations and are about 5000 rad/rad and $4 \text{ pm}/\mu\text{rad}$, including some initial interferometric misalignment of about $50 \mu\text{rad}$. The projected tilt noise is shown by the dotted black line plotted in Fig. 3. It matches the residual phase noise, \tilde{x}_{RPN} , above 200 mHz and might explain some of the noise increase below 200 mHz. Not measured here are beam pointing fluctuations of the reference interferometer which likely also drive the performance of \tilde{x}_{RPN} by coupling into the measurement via residual noise of the laser frequency stabilisation [25]. This could explain the missing correlation between projected tilt noise and residual phase noise measurement at low frequencies.

IV. SUMMARY

The usage of deep frequency modulation interferometry (DFMI) allows simpler laser preparation in comparison to heterodyne interferometry. It can further maintain

multi-fringe capabilities that are required, for example, for a TM readout in space. Only one frequency reference interferometer is required per laser source. The so-prepared laser light can be distributed into many optical set-ups whose number is finally constrained by the minimal optical power required not to be limited by shot noise.

Using a compact, single-component beam splitting and recombination optic specifically designed for DFMI we conducted a prototype test mass experiment in which we were able to reach displacement sensing levels of $230 \text{ fm}/\sqrt{\text{Hz}}$ around 300 mHz and tilt noise readouts with sensitivities of about $20 \text{ nrad}/\sqrt{\text{Hz}}$ at 40 mHz. The current performance limitation at low frequencies is most probably caused by beam pointing fluctuations which can be reduced by using ultra-stable, monolithic fiber output couplers in future experiments. At high frequencies we are currently limited by the digitisation noise of our data acquisition system. The required strong frequency modulation causes non-linearities which were discussed and found not to be limiting in the dynamic range regime probed here. Future work will concentrate on the development of scalable phasemeters with many channels and on optimising the readout and laser control algorithms to further test and increase the phase readout linearity. The experiment represented here is a well-suited testbed for these future investigations.

To conclude, the simplicity of the compact interferometric setup and the achieved LISA-like performance make deep frequency modulation interferometry attractive for future experiments and metrology applications.

ACKNOWLEDGMENTS

The authors would like to thank the DFG Sonderforschungsbereich (SFB) 1128 Relativistic Geodesy and Gravimetry with Quantum Sensors (geo-Q) and the International Max-Planck Research School (IMPRS) for financial support.

-
- [1] B. P. Abbott, R. Abbott, T. Abbott, F. Acernese, K. Ackley, C. Adams, T. Adams, P. Addesso, R. Adhikari, V. Adya, *et al.*, *Physical review letters* **119**, 141101 (2017).
 - [2] T. S. Schwarze, G. Fernández Barranco, D. Penkert, M. Kaufer, O. Gerberding, and G. Heinzel, *Phys. Rev. Lett.* **122**, 081104 (2019).
 - [3] K. Danzmann *et al.*, arXiv preprint arXiv:1702.00786 (2017).
 - [4] M. Armano, H. Audley, J. Baird, P. Binetruy, M. Born, D. Bortoluzzi, E. Castelli, A. Cavalleri, A. Cesarini, A. Cruise, *et al.*, *Physical Review Letters* **120**, 061101 (2018).
 - [5] M. R. Drinkwater, R. Haagsmans, D. Muzi, A. Popescu, R. Floberghagen, M. Kern, and M. Fehringer, in *Proceedings of the 3rd international GOCE user workshop* (European Space Agency Noordwijk, The Netherlands, 2006) pp. 6–8.
 - [6] K. Douch, H. Wu, J. Müller, and G. Heinzel, in *IAG Workshop, Bonn, Germany* (2017).
 - [7] J. Watchi, S. Cooper, B. Ding, C. M. Mow-Lowry, and C. Collette, *Review of Scientific Instruments* **89**, 121501 (2018).
 - [8] D. A. Shaddock, *Optics letters* **32**, 3355 (2007).
 - [9] T. S. Schwarze, O. Gerberding, F. G. Cervantes, G. Heinzel, and K. Danzmann, *Optics express* **22**, 18214 (2014).
 - [10] G. Heinzel, F. Guzmán Cervantes, A. F. Garcia Marin,

- J. Kullmann, W. Feng, and K. Danzmann, *Optics express* **18**, 19076 (2010).
- [11] O. Gerberding, *Optics Express* **23**, 14753 (2015).
- [12] K.-S. Isleif, O. Gerberding, M. Mehmet, T. S. Schwarze, G. Heinzl, and K. Danzmann, *Journal of Physics: Conference Series* **716**, 012008 (2016).
- [13] K.-S. Isleif, O. Gerberding, T. S. Schwarze, M. Mehmet, G. Heinzl, and F. G. Cervantes, *Opt. Express* **24**, 1676 (2016).
- [14] A. J. Sutton, O. Gerberding, G. Heinzl, and D. A. Shaddock, *Optics express* **20**, 22195 (2012).
- [15] K.-S. Isleif, O. Gerberding, S. Köhlenbeck, A. Sutton, B. Sheard, S. Gößler, D. Shaddock, G. Heinzl, and K. Danzmann, *Optics express* **22**, 24689 (2014).
- [16] T. Kissinger, T. O. H. Charrett, and R. P. Tatam, *Measurement Science and Technology* **24**, 094011 (2013).
- [17] T. Kissinger, T. O. Charrett, and R. P. Tatam, *Optics express* **23**, 9415 (2015).
- [18] G. De Vine, D. S. Rabeling, B. J. Slagmolen, T. T. Lam, S. Chua, D. M. Wuchenich, D. E. McClelland, and D. A. Shaddock, *Optics express* **17**, 828 (2009).
- [19] S. A. Akbarzadeh-Jahromi and M. Shahabadi, *IEEE Sensors Journal* **17**, 5460 (2017).
- [20] C. Ni, M. Zhang, Y. Zhu, C. Hu, S. Ding, and Z. Jia, *Appl. Opt.* **56**, 3895 (2017).
- [21] M. Zhang, C. Ni, Y. Zhu, L. Wang, C. Hu, and J. Hu, *Chin. Opt. Lett.* **15**, 101201 (2017).
- [22] M. Arablu and S. T. Smith, *Review of Scientific Instruments* **89**, 055007 (2018).
- [23] S. Cooper, C. Collins, A. Green, D. Hoyland, C. Speake, A. Freise, and C. Mow-Lowry, *Classical and Quantum Gravity* **35**, 095007 (2018).
- [24] G. Wanner, G. Heinzl, E. Kochkina, C. Mahrtdt, B. S. Sheard, S. Schuster, and K. Danzmann, *Optics Communications* **285**, 4831 (2012).
- [25] O. Gerberding, K.-S. Isleif, M. Mehmet, K. Danzmann, and G. Heinzl, *Physical Review Applied* **7**, 024027 (2017).
- [26] G. Heinzl, V. Wand, A. Garcia, O. Jennrich, C. Braxmaier, D. Robertson, K. Middleton, D. Hoyland, A. Rüdiger, R. Schilling, *et al.*, *Classical and Quantum Gravity* **21**, S581 (2004).
- [27] G. de Vine, B. Ware, K. McKenzie, R. E. Spero, W. M. Klipstein, and D. A. Shaddock, *Physical review letters* **104**, 211103 (2010).
- [28] T. Schuldt, M. Gohlke, H. Kögel, R. Spannagel, A. Peters, U. Johann, D. Weise, and C. Braxmaier, *Measurement Science and Technology* **23**, 054008 (2012).
- [29] F. G. Cervantes, R. Flatscher, D. Gerardi, J. Burkhardt, R. Gerndt, M. Nofrarias, J. Reiche, G. Heinzl, K. Danzmann, L. G. Boté, *et al.*, in *APS Conf Ser*, Vol. 467 (2013) pp. 141–150.